

Myosin-dependent actin stabilization as revealed by single-molecule imaging of actin turnover

Sawako Yamashiro^{a,b,†,*}, Soichiro Tanaka^{c,†}, Laura M. McMillen^d, Daisuke Taniguchi^b, Dimitrios Vavylonis^d, and Naoki Watanabe^{a,b}

^aLaboratory of Single-Molecule Cell Biology, Kyoto University Graduate School of Biostudies, and ^bDepartment of Pharmacology, Kyoto University Graduate School of Medicine, Kyoto 606-8501, Japan; ^cLaboratory of Single-Molecule Cell Biology, Tohoku University Graduate School of Life Sciences, Sendai, Miyagi 980-8578, Japan; ^dDepartment of Physics, Lehigh University, Bethlehem, PA 18015

ABSTRACT How mechanical stress applied to the actin network modifies actin turnover has attracted considerable attention. Actomyosin exerts the major force on the actin network, which has been implicated in actin stability regulation. However, direct monitoring of immediate changes in F-actin stability on alteration of actomyosin contraction has not been achieved. Here we reexamine myosin regulation of actin stability by using single-molecule speckle analysis of actin. To avoid possible errors attributable to actin-binding probes, we employed DyLight-labeled actin that distributes identical to F-actin in lamellipodia. We performed time-resolved analysis of the effect of blebbistatin on actin turnover. Blebbistatin enhanced actin disassembly in lamellipodia of fish keratocytes and lamellar of *Xenopus* XTC cells at an early stage of the inhibition, indicating that actomyosin contraction stabilizes cellular F-actin. In addition, our data show a previously unrecognized relationship between the actin network-driving force and the actin turnover rates in lamellipodia. These findings point to the power of direct viewing of molecular behavior in elucidating force regulation of actin filament turnover.

Monitoring Editor

Valerie Marie Weaver
University of California,
San Francisco

Received: Jan 26, 2018

Revised: May 21, 2018

Accepted: May 23, 2018

INTRODUCTION

Cells reorganize the actin cytoskeleton in response to internal and external forces. Accumulating biochemical evidence of actin filaments implies that actin filaments themselves may act as mechanosensors (Galkin *et al.*, 2012; Hayakawa *et al.*, 2012; Romet-Lemonne and Jegou, 2013). In vitro, tension in an isolated actin filament prevents severing by the key actin depolymerization regulator cofilin (Hayakawa *et al.*, 2011), whereas myosin promotes disassembly of

actin filaments (Haviv *et al.*, 2008; Murrell and Gardel, 2012; Reymann *et al.*, 2012; Vogel *et al.*, 2013). In cells, actin remodeling induced by external forces has been reported. For instance, unidirectional cyclic stretch induces reorientation of actin stress fibers and cell alignment perpendicular to the stretch axis (Shirinsky *et al.*, 1989; Kaunas *et al.*, 2005; Hoffman *et al.*, 2012; Greiner *et al.*, 2013). In fast migrating fish keratocytes, cyclic stretch induces migration parallel to the direction of stretch concomitantly with reorientation of stress fibers (Okimura and Iwadate, 2016). Brief deformation of the cell cortex rapidly increases G-actin, which in turn triggers frequent actin nucleation by formin homology proteins (Higashida *et al.*, 2013). Although how mechanical stress modifies actin stability has been one of the key questions, direct monitoring immediate changes in F-actin stability on alteration of forces has not yet been achieved in cells.

Single-molecule speckle (SiMS) microscopy is a powerful approach to elucidate the rapid change in actin turnover on pharmacological treatments. In SiMS, appearance and disappearance of fluorescently labeled single-molecule actin speckles directly report actin assembly and disassembly (Watanabe and Mitchison, 2002). We recently developed an electroporation-based SiMS method called eSiMS (Yamashiro *et al.*, 2014, 2015; Yamashiro and Watanabe, 2017). In the method, electroporation-mediated delivery of DyLight550-actin (DL-actin) into cells enables us to label cells with

This article was published online ahead of print in MBcC in Press (<http://www.molbiolcell.org/cgi/doi/10.1091/mbc.E18-01-0061>) on May 30, 2018.

[†]These authors contributed equally.

*Address correspondence to: Sawako Yamashiro (yamashiro.sawako.5c@kyoto-u.ac.jp).

Author contributions: S. Y. and S. T. performed experiments and analyzed data. S. Y., S. T., and N. W. designed experiments. L. M. M., D. T., D. V., and N. W. performed simulations. S. Y., D. V., and N. W. wrote the manuscript; all other authors edited the manuscript.

Abbreviations used: DL, DyLight; EMCCD, electron-multiplying charge-coupled device; eSiMS, electroporation-based single-molecule speckle microscopy; FRAP, fluorescence recovery after photobleaching; PAF, photoactivation of fluorescence; qFSM, quantitative fluorescent speckle microscopy; SiMS, single-molecule speckle.

© 2018 Yamashiro, Tanaka, *et al.* This article is distributed by The American Society for Cell Biology under license from the author(s). Two months after publication it is available to the public under an Attribution–Noncommercial–Share Alike 3.0 Unported Creative Commons License (<http://creativecommons.org/licenses/by-nc-sa/3.0>).

“ASCB®,” “The American Society for Cell Biology®,” and “Molecular Biology of the Cell®” are registered trademarks of The American Society for Cell Biology.

100% efficiency at the optimal low density, which expands applications to primary cells. This allows us to employ migrating keratocytes in the present study for direct monitoring of the early effect of myosin II inhibitor blebbistatin (Straight *et al.*, 2003) on F-actin stability. In addition, DL-actin provides substantially improved brightness and photostability (Yamashiro *et al.*, 2014). The slow photobleaching of DL-actin enables simultaneous lifetime measurement of actin populations with distinct disassembly kinetics.

Several previous studies have investigated myosin regulation of F-actin stability in live cells. During cytokinesis, blebbistatin has been reported either to delay (Guha *et al.*, 2005; Murthy and Wadsworth, 2005) or to promote disassembly (Kondo *et al.*, 2012) of the contractile actin ring. In neuronal growth cones, myosin II promotes compression and severing of actin bundles (Medeiros *et al.*, 2006). The protein phosphatase inhibitor calyculin A, which was used to manipulate myosin activity, has been reported to increase actin network disassembly in lamella of epithelial cells (Vallotton *et al.*, 2004). Wilson *et al.* (2010) reported that actin-myosin II contraction enhances actin network disassembly in migrating fish keratocytes. However, such previous live cell experiments may have three potential methodological problems as follows.

First, the use of indirect actin probes or fluorescent protein-tagged actin may have hampered monitoring whole actin populations. In live cells, phalloidin and Lifeact misdistribute toward the rear of lamellipodia via a convection-induced mechanism (unpublished data). In addition, phalloidin competes with cofilin for binding to F-actin (Nishida *et al.*, 1987), causing oversight of fast depolymerizing F-actin species. Furthermore, phalloidin may stabilize its bound F-actin locally and disturb actin turnover measurement. For example, Wilson *et al.* (2010) employed fluorescent phalloidin as an F-actin probe in quantitative fluorescent speckle microscopy (qFSM) in live keratocytes. Their main finding was a high net decrease in F-actin mass along the actin flow in the rear of the cell where myosin II accumulates. This result may have been severely influenced by the discrepancy between phalloidin and F-actin localization.

The use of fluorescent protein-tagged actin might have also partially hindered observation of the formin-based actin dynamics due to their interference with formins (Chen *et al.*, 2012; Yi *et al.*, 2012; Yamashiro *et al.*, 2014; Murugesan *et al.*, 2016). For example, actin turnover in the contractile actin ring of cultured cells have been measured by fluorescence recovery after photobleaching (FRAP) with GFP-actin (Murthy and Wadsworth, 2005) or mCherry-actin (Kondo *et al.*, 2012). However, formin mDia2 localizes to the cleavage furrow and induces F-actin scaffold for the contractile ring in the cytokinesis of several cell types (Watanabe *et al.*, 2008). In addition, GFP-actin is not suited for combination with blebbistatin, which exhibits phototoxicity on cells and loses its activity on blue light irradiation (Kolega, 2004; Sakamoto *et al.*, 2005).

Second, the direct effect of blebbistatin may have not been monitored adequately. Blebbistatin's effect in blocking cellular myosin II-dependent contraction are noticeable within ~2 min (Straight *et al.*, 2003; Yamashiro *et al.*, 2014). In case actomyosin contractile force stabilizes a certain population of F-actin, it is critical to capture initial response to the blebbistatin treatment because such F-actin may disappear rapidly and measuring the turnover of remaining F-actin may lead to different conclusions depending on the turnover rate of the remaining F-actin. Thus, in previous live cell experiments where actin turnover measurements by FRAP (Guha *et al.*, 2005; Kondo *et al.*, 2012) or qFSM (Wilson *et al.*, 2010) were performed 10 min to 2 h after the addition of blebbistatin, the initial response to inhibition of myosin-based contractility might have been missed. In addition, Guha *et al.* (2005) and Kondo *et al.* (2012) performed

FRAP analyses for actin in the contractile ring that had been formed in the presence of blebbistatin. This may alter configuration and thereby dynamics of the contractile ring.

Apart from blebbistatin, Vallotton *et al.* (2004) used calyculin A to manipulate myosin activity. However, calyculin A, a broad inhibitor against protein phosphatase 2A and protein phosphatase 1, affects on phosphorylation status of many proteins including Rho GTPase-activating protein FilGAP (Morishita *et al.*, 2015) and focal adhesion proteins (p125^{Fak}, p130^{Cas} and paxillin) (Leopoldt *et al.*, 2001). Therefore, the effect of calyculin A is not limited to myosin phosphatase.

Third, in many previous studies, F-actin turnover was inferred from indirect measurements that report the combined effects of actin assembly, disassembly, and transport of many actin filaments rather than individual actin monomers disassembly. Vallotton *et al.* (2004) and Wilson *et al.* (2010) presented qFSM results for the net actin decrease on the calyculin A treatment (Vallotton *et al.*, 2004) and along the actin flow (Wilson *et al.*, 2010), respectively. However, since actin assembly and disassembly occur simultaneously, one cannot directly derive the actin disassembly rate from the net actin decrease. In neuronal growth cones, it remains unclear whether compression and severing of actin bundles by myosin II (Medeiros *et al.*, 2006) are accompanied by enhanced actin disassembly. For these reasons, myosin-mediated contractile force regulation of actin turnover *in vivo* has remains to be examined.

In this study, we performed time-resolved analysis of the effect of blebbistatin on actin turnover using eSIMS microscopy. We employed the DL-actin probe, which retains the ability to collaborate with mDia1 and mDia2 *in vitro* (Yamashiro *et al.*, 2014; Mizuno *et al.*, 2018). The distribution of DL-actin is compatible with F-actin distribution in lamellipodia of keratocytes (unpublished data). Our data indicate that actomyosin contraction stabilized on F-actin in lamellipodia and lamella. In addition, we find that cell migration speeds are negatively correlated with the actin turnover rates in lamellipodia of keratocytes. These findings with direct observation of actin turnover at the molecular level provides new insights into actin dynamics and myosin function in cell migration.

RESULTS AND DISCUSSION

Direct observation of actin turnover by single-molecule imaging in live keratocytes

DyLight550-actin (DL-actin) was delivered into the cytoplasm of fish keratocytes by electroporation (Figure 1A and Supplemental Video 1) (Yamashiro *et al.*, 2014, 2015). The distribution of DL-actin speckles in lamellipodia was consistent with F-actin distribution in the previous studies (Theriot and Mitchison, 1991; Svitkina *et al.*, 1997). In marked contrast, fluorescent phalloidin showed rear-biased misdistribution in both XTC cells (Supplemental Figure S1, A and B) and keratocytes (Supplemental Figure S1D). The detailed comparison between fluorescently labeled actin, phalloidin, and Lifeact and the underlying mechanism of the misdistribution of F-actin binding probes will be reported elsewhere (unpublished data). These results suggest that phalloidin is not suitable to monitor actin assembly and disassembly in lamellipodia of live cells.

DL-actin SIMS reported that the majority of actin assembly occurred at the leading edge of lamellipodia (Figure 1B, left). Actin assembly was also observed throughout lamellipodia as is the case with XTC cells (Watanabe and Mitchison, 2002). In contrast, actin disassembly was observed evenly in lamellipodia (Figure 1B, right). These findings differ from the previous report by Wilson *et al.* (2010), who concluded that disassembly is localized at the rear of keratocytes.

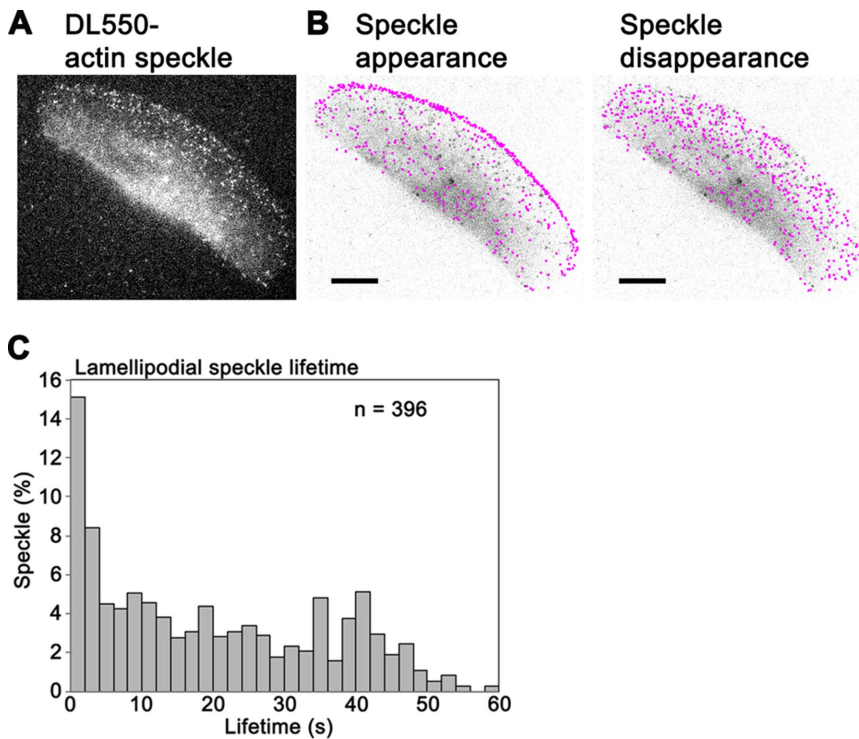


FIGURE 1: (A) Live image of DyLight550-actin (DL-actin) speckles in a keratocyte with epifluorescence microscopy. (B) Positions of appearance of DL-actin speckles in a 34-s time window (left) and disappearance of these speckles (right) are indicated by pink dots over an image of the keratocyte. Bars, 10 μm . (C) Lifetime distribution of DL-actin speckles in lamellipodia of keratocytes.

Lifetime analysis showed that 37% of F-actin subunits depolymerize within 10 s after polymerization (Figure 1C). This fast actin turnover cannot be explained by the treadmilling model (Small, 1995). Our data confirm fast actin turnover in lamellipodia of keratocytes, which was proposed in the photoactivation of fluorescence (PAF) study (Theriot and Mitchison, 1991). The average half-life of F-actin was 12.6 ± 3.5 s in keratocytes ($n = 14$ cells, mean \pm SD), which is almost half the previously reported half-life of F-actin, 23 s (Theriot and Mitchison, 1991). These discrepancies may arise from the difference in the spatial resolution between PAF and SiMS. The decay rate in PAF and FRAP does not necessarily represent F-actin disassembly rate under certain conditions (Tardy *et al.*, 1995). Using the Tardy model, we previously estimated that the local reincorporation mechanism may retard the apparent PAF decay approximately two times slower than true actin disassembly in XTC cells (Watanabe and Mitchison, 2002; Watanabe, 2010). We further elaborated on this effect with a model that accounts for the spatially dependent speckle appearance and lifetime distribution, both revealed by SiMS (Smith *et al.*, 2013). We used this model to perform PAF simulations based on our keratocyte SiMS data of DL-actin. In the simulated intensity decay curves, rapid decay immediately after $t = 0$ is mainly due to the diffusion of G-actin (Supplemental Figure S2C). An exponential fit to the portions of the curves extending beyond 5 s, which excludes the influence of the diffusion of G-actin, corresponds to the half-time value of 32 s, which is larger compared with the implemented bound particle half-time of 15 s (see Supplemental Figure S2C and Supplemental Method). These results confirm that the actin disassembly rate measured by PAF and FRAP may become slower than the true actin disassembly rate in lamellipodia of keratocytes.

The discrepancy may also arise from the difference in the experimental conditions as the PAF experiments were performed at 15°C

to slow cell movement less than 10 $\mu\text{m}/\text{min}$ (Theriot and Mitchison, 1991) while we performed SiMS imaging at room temperature, 21–23°C. At 15°C, the migration speeds of keratocytes from *Gillichthys mirabilis* and *Cyprinodon salinus* are reduced only to 70–80% of the speeds at 20°C (Ream *et al.*, 2003). We therefore predict that the local reincorporation mechanism may in part account for the delayed decay rates in the PAF study (Theriot and Mitchison, 1991). These findings point to the importance of direct viewing of molecular behavior.

Myosin contractile force stabilizes F-actin in pseudopodia

We reevaluated myosin regulation of F-actin stability by using eSiMS microscopy for time-resolved analysis of the effect of blebbistatin on actin turnover in keratocytes. We first addressed the timing of actomyosin inhibition by blebbistatin. As shown in a previous study (Straight *et al.*, 2003), the shape of keratocytes expanded laterally within 2 min after perfusion of blebbistatin (Figure 2, A and B, and Supplemental Video 2). The trajectories of actin speckles, which were biased toward the centerline in untreated cells, became parallel to the direction of cell migration 90 s after the blebbistatin treatment (Figure 2C). On the basis of these observations, we predicted that actomyosin contraction was inhibited as early as 90 s after the blebbistatin treatment.

We then compared DL-actin speckle regression kinetics before and after the blebbistatin treatment. Since the keratocyte is thick at the rear and its cell body rotates during locomotion (Anderson *et al.*, 1996), we first checked three-dimensional movement of DL-actin speckles by using dual-focus imaging optics (Watanabe *et al.*, 2007). Among the actin speckles that disappeared in the perinuclear and the rear regions of the cell, ~12% moved from the lower focal plane toward the upper focal plane before disappearance (14 of 115 speckles; data not shown). It was not feasible to distinguish actin disassembly from moving away of speckles from the focal plane using our current optics. Therefore, we limited speckle regression kinetics analysis in thin lamellipodia to track all actin speckles in focus.

The dissociation rate of actin SiMS increased by 29% on blebbistatin treatment (0.058 ± 0.017 s⁻¹ to 0.074 ± 0.022 s⁻¹, mean \pm SD, $p < 0.05$, two-tailed paired *t* test), whereas the dissociation rate increased by only 10% in mock-treated cells (0.063 ± 0.014 s⁻¹ to 0.070 ± 0.016 s⁻¹, $p < 0.05$, two-tailed paired *t* test) (Figure 2D). Thus under the condition where excitation light can be strongly attenuated for bright DL-actin probes, long-term SiMS image acquisition may accelerate actin disassembly to a small degree. Nonetheless, the increase in the actin SiMS dissociation rate was much larger (29%) in blebbistatin-treated cells than in mock-treated cells (10%). These results indicate that blebbistatin accelerates actin disassembly in keratocytes.

We also found similar effects of blebbistatin in XTC cells. Blebbistatin slows the retrograde actin flow in lamella but not in lamellipodia of XTC cells, accompanied by disintegration of lamellar actin bundles, which takes place 1–2 min after drug perfusion (Yamashiro *et al.*, 2014). We therefore examined the effect of blebbistatin in the lamella region of XTC cells (Figure 3A). We confirmed that the

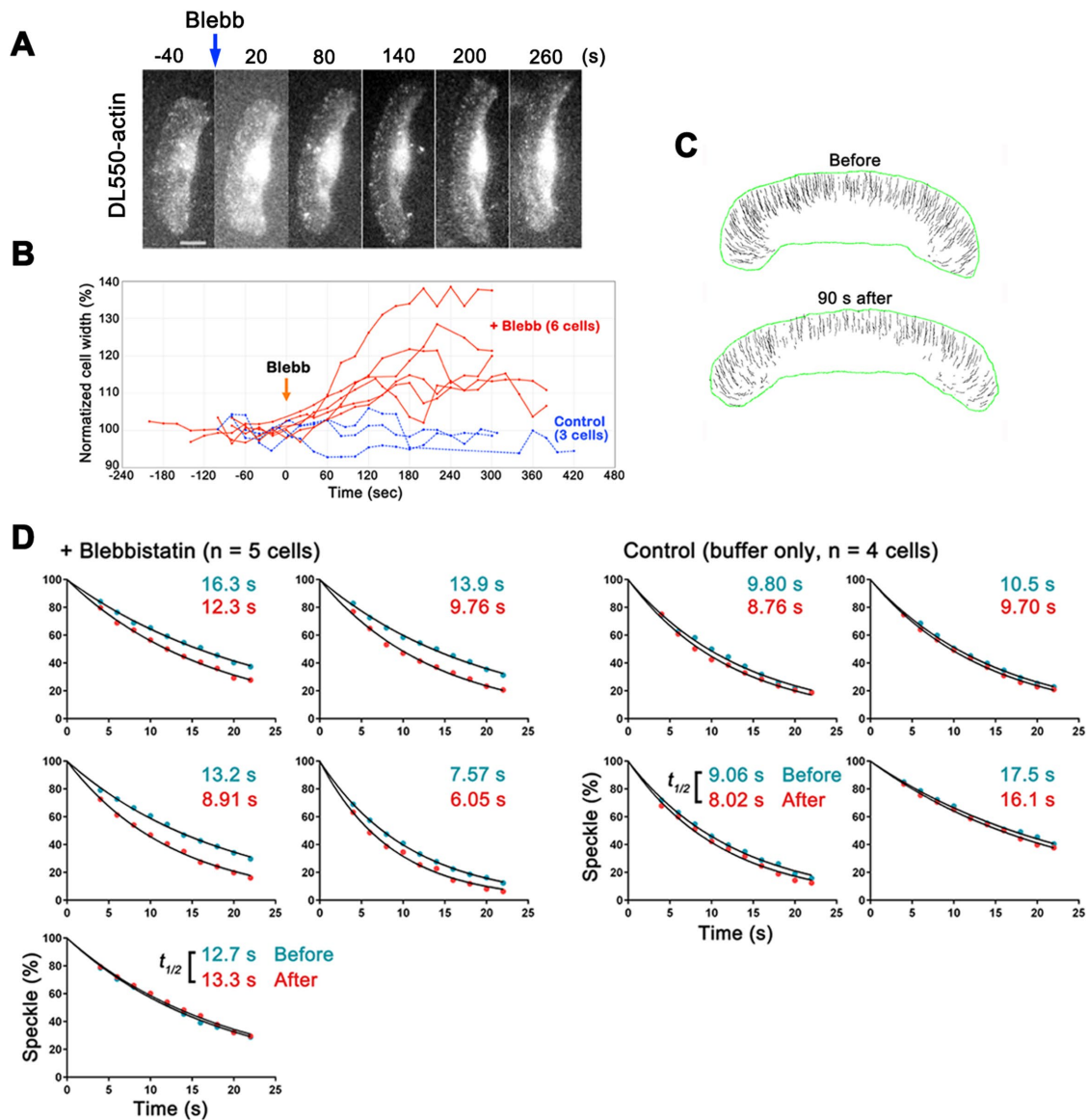


FIGURE 2: Blebbistatin enhanced actin disassembly in lamellipodia of keratocytes. (A) Time-lapse images of a keratocyte loaded with DL-actin at 60-s intervals. Blebbistatin (50 μ M) was added at 0 s. (B) The graph shows variations in the normalized cell width (%) of blebbistatin-treated keratocytes (red lines) and control cells (blue lines). Blebbistatin induced lateral expansion of keratocytes within 2 min. (C) Trajectories of speckles before and 90 s after the blebbistatin treatment. (D) Regression measurements of DL-actin speckles in lamellipodia of keratocytes before (blue dots) and after (red dots) treatment with 50 μ M blebbistatin (left). Images were acquired at 2-s intervals. The data were normalized for photobleaching (Watanabe and Mitchison, 2002; Yamashiro *et al.*, 2014). For the regression analysis of DL-actin speckles after the treatment, the first frame of the analysis is within 90–180 s after adding blebbistatin. Right, control cells. The single exponential curve (black lines) fitted to the data gave half-life of speckles ($t_{1/2}$). The dissociation rate of actin speckles was significantly higher in the cells after the blebbistatin treatment than that in the cells before the treatment ($p < 0.05$, two-tailed paired t test).

average speed of speckles in lamella were decelerated 70 s after the blebbistatin treatment (Figure 3B, and Supplemental Table S1) and found that blebbistatin destabilized long-lived population of lamellar F-actin (Figure 3C). In this analysis, we only compared the regression rates of the DL-actin speckles which survived over 40 s, because we noticed that the number of short-lived DL-actin speckles (half-life, ≈ 32 s) (Yamashiro *et al.*, 2014) greatly fluctuates over time. Blebbistatin treatment increased the dissociation rate of long-lived actin SiMS by 77% (Figure 3C). The dissociation rate of actin SiMS (mean \pm SD) was 0.011 ± 0.0026 s^{-1} before blebbistatin and 0.019 ± 0.0073 s^{-1} after blebbistatin ($p < 0.05$). Furthermore, blebbistatin

increased the frequency of actin nucleation by formin mDia1 (Supplemental Figure S3), suggesting that blebbistatin-induced G-actin release contributes to enhanced formin-mediated actin nucleation (Higashida *et al.*, 2004; Higashida *et al.*, 2013). These results indicate that actomyosin contractile force stabilizes cellular F-actin in XTC cells.

Taken together, our direct observations unambiguously revealed that actomyosin contractile force stabilizes actin filament in lamellipodia and lamella. Myosin II-dependent tension may prevent F-actin from being severed by cofilin as previously shown *in vitro* (Hayakawa *et al.*, 2011). Our results suggest that the cellular

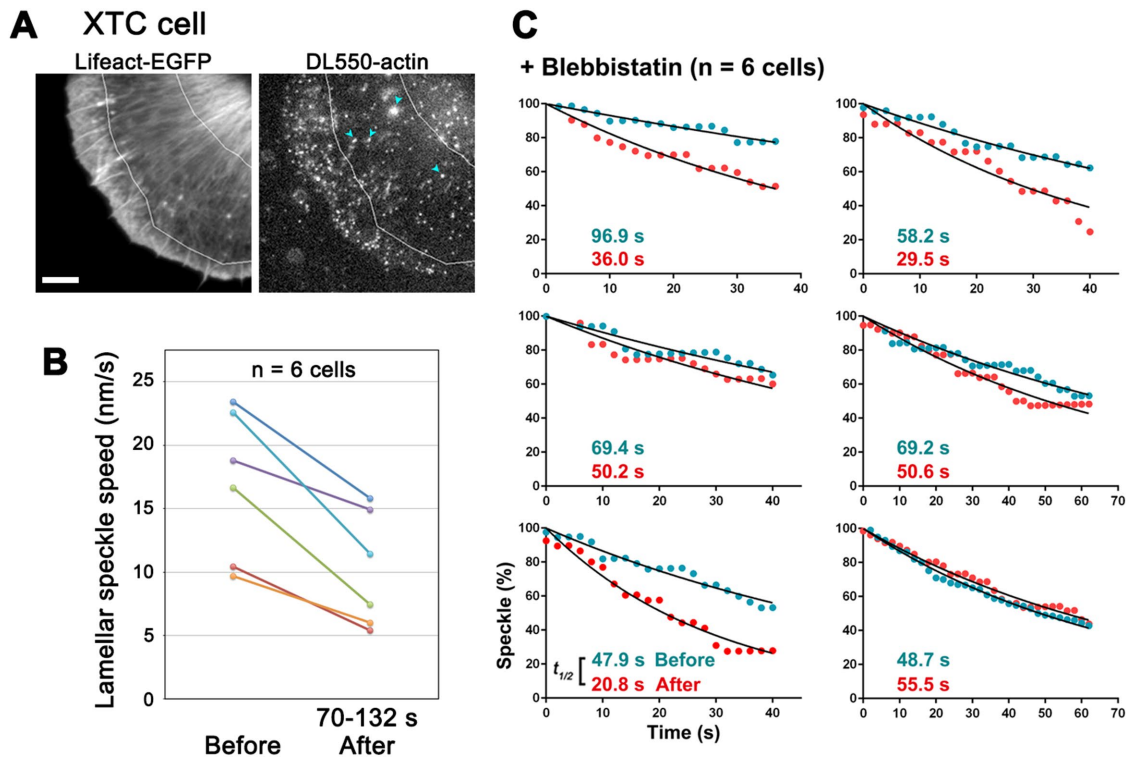


FIGURE 3: Blebbistatin enhanced actin disassembly in lamella of XTC cells. (A) Live images of Lifact-EGFP (left) and DL-actin speckles (right) in a XTC cell. DL-actin speckles in the lamellar region between two white lines were analyzed. Blue arrows indicate fluorescent organelle-like structures, which is apparently an artifact of electroporation. Bar, 5 μ m. (B) The retrograde flow speeds in lamella before and 70–132 s after the 50 μ M blebbistatin treatment. Each colored line represents data from an individual cell (n = 6 cells). The retrograde flow speeds at each point show the average speeds of 10 actin speckles in lamella. (C) Regression measurements of long-lived population of DL-actin speckles (Yamashiro *et al.*, 2014) in lamella of XTC cells before (blue dots) and 70–132 s after (red dots) the blebbistatin treatment. To evaluate long-lived population of DL-actin speckles, speckles that exist at least 40 s were measured. The dissociation rate of long-lived actin speckles was significantly higher in the cells after the blebbistatin treatment than that in the cells before the treatment ($p < 0.05$, two-tailed paired *t* test).

actin filaments pulled by actomyosin contractile force become stabilized rather than being prone to disassembly, which presumably facilitates effective force transduction within the actin filament network.

Actin turnover rates correlate with speeds of cell migration and retrograde actin flow in keratocytes

In addition, we found another relationship between the actin network-driving force and the actin turnover rate in lamellipodia of keratocytes. Interestingly, the faster the cell migrates, the faster the actin turnover rate is in the lamellipodium (Figure 4A, blue dots). This correlation suggests the existence of a cell speed acceleration mechanism involving enhancement of actin turnover. Treatment of keratocytes with blebbistatin changed neither cell speed nor the speed of the retrograde actin flow with respect to the cell edge 90–240 s after the treatment (data not shown), suggesting that this acceleration mechanism is independent of myosin II activities.

By using SiMS microscopy, actin was found to flow inward with respect to the substratum at 10–60 nm/s (Figure 4, B and C) as previously reported in fluorescent speckle microscopy studies (Jurado *et al.*, 2005; Schaub *et al.*, 2007). The slow backward actin flow with respect to the substratum may have been overlooked by the PAF analysis (Theriot and Mitchison, 1991) due to its limited spatial resolution. SiMS analysis revealed that fast retrograde actin flow rates with respect to the substratum tend to be associated with fast actin

turnover rates (Figure 4A, red dots). Strengthening linkage between cell adhesion molecules and the actin network slows the retrograde actin flow as proposed in the clutch model (Mitchison and Kirschner, 1988). We therefore predict that in cells with slow actin flow, the actin network is strongly engaged to cell adhesions and tension exerted by the retrograde actin flow would mount in F-actin. This could account for the association between fast retrograde actin flow rates with respect to the substratum and fast actin turnover rates.

In summary, our study revealed that actomyosin contraction stabilizes F-actin in lamellipodia and lamella, providing the direct evidence of F-actin stabilization by tensile force *in vivo*. This conclusion agrees with the *in vitro* study by Hayakawa *et al.* (2011). In epithelial cells, blebbistatin has been reported to induce disintegration of peripheral actomyosin bundles, accompanied by increase in G-actin levels in cytoplasm (Lomakin *et al.*, 2015). Although it remains unclear whether blebbistatin promotes actin disassembly or inhibits the formation of epithelial actomyosin bundles, myosin-mediated contractile force appears to contribute to F-actin stabilization also in epithelial cells. To reconcile the opposite conclusions between our study and the previous studies (Vallotton *et al.*, 2004; Guha *et al.*, 2005; Medeiros *et al.*, 2006), we speculate that myosin-derived force may either stabilize F-actin by imposing tensile force or destabilize F-actin by compression depending on the actomyosin architecture. Furthermore, our SiMS analysis revealed a negative correlation between cell migration speeds and the actin turnover rates (but

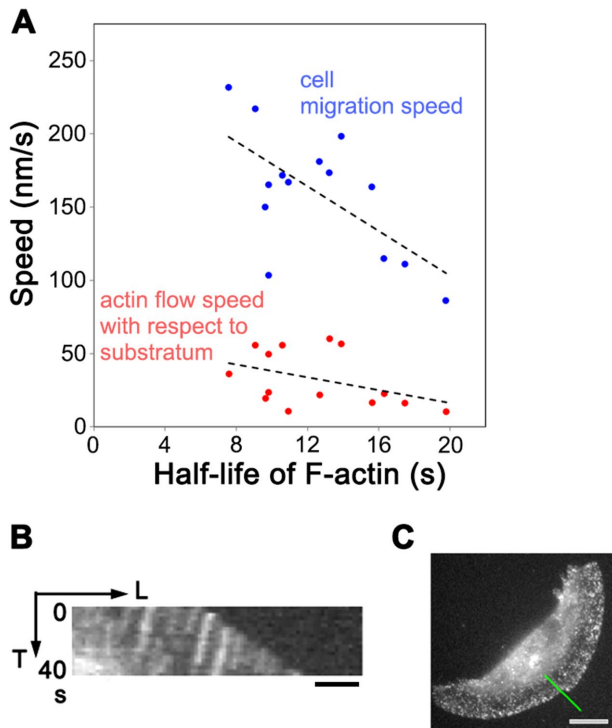


FIGURE 4: (A) Relationship between the half-life of lamellipodial actin filaments and cell migration speed (blue dots, Pearson correlation coefficient, $r = -0.623$, $p = 0.0172$) or actin flow speed with respect to substratum (red dots, $r = -0.402$, $p = 0.154$) in individual keratocytes. (B) Kymograph of actin speckles at the cell periphery showing retrograde actin flow toward the cell center with respect to the substratum. Bar, 2 μm . The line in C indicates the region for the kymograph. Bar, 10 μm .

not the rate of treadmilling) in keratocytes. Direct visualization of molecular behavior provides critical information for our precise understanding of the molecular remodeling mechanisms in complex biological systems.

MATERIALS AND METHODS

Fluorescent dye-labeled actin

Rabbit skeletal muscle actin labeled with DyLight550-NHS ester (Thermo Fisher Scientific) was prepared as described previously (Yamashiro *et al.*, 2014).

Cell culture and electroporation

Keratocytes were isolated from scales of goldfish (*Carassius auratus*) by culturing between a culture dish and a coverslip, using the keratocyte culture medium composed of L-15 Leibovitz medium (Invitrogen), 10% fetal bovine serum (Nichirei Biosciences), and 1% Antibiotic-Antimycotic Mixed Stock Solution (Nacalai Tesque). Then keratocytes were trypsinized, resuspended with the culture medium, collected by centrifugation, and subjected for electroporation to deliver DL550-actin as described (Yamashiro *et al.*, 2014). *Xenopus laevis* XTC cells were maintained as described previously (Watanabe and Mitchison, 2002; Watanabe, 2012). DL-actin was electroporated into XTC cells as described (Yamashiro *et al.*, 2014).

Single-molecule speckle imaging and data analysis

SIMS imaging with epifluorescence microscopy was carried out as described previously (Watanabe, 2012; Yamashiro *et al.*, 2015). Keratocytes were seeded on a coverslip in the keratocyte culture

medium excluded riboflavin and phenol red to reduce the fluorescence background. XTC cells were allowed to spread on a poly-L-lysine-coated coverslip in 70% L-15 Leibovitz medium without serum, riboflavin, and phenol red. Imaging was performed using a microscope (IX71, Olympus) equipped with a PlanApo 1.40 NA 100 \times oil objective (Olympus), 100-W mercury illumination, and a cooled electron-multiplying charge-coupled device (EMCCD) camera (Evolve 512, Photometrics). A TRITC-A-Basic filter set (Semrock) was used for imaging DL-actin. Speckles were analyzed by using Speckle TrackerJ as described (Yamashiro *et al.*, 2014, 2015). The data of regression analysis and lifetime analysis were normalized for photobleaching (Watanabe and Mitchison, 2002; Watanabe, 2012). (S)-(-)-blebbistatin (Tronto Research Chemicals) was applied to the cells at a final concentration of 50 μM .

ACKNOWLEDGMENTS

We thank Ayako Kodera and Shuh Yamamura for help with SIMS analysis. This work was supported by Japan Society for the Promotion of Science (JSPS) KAKENHI Grant Number JP15K07045 (S.Y.), by National Institutes of Health RO1GM114201 (D.V.), by Japan Science and Technology Agency (JST)-CREST Grant Number JPM-JCR15G5 (N.W.), and by the Uehara Memorial Foundation (N.W.).

REFERENCES

- Anderson KI, Wang YL, Small JV (1996). Coordination of protrusion and translocation of the keratocyte involves rolling of the cell body. *J Cell Biol* 134, 1209–1218.
- Chen Q, Nag S, Pollard TD (2012). Formins filter modified actin subunits during processive elongation. *J Struct Biol* 177, 32–39.
- Galkin VE, Orlova A, Egelman EH (2012). Actin filaments as tension sensors. *Curr Biol* 22, R96–R101.
- Greiner AM, Chen H, Spatz JP, Kemkemer R (2013). Cyclic tensile strain controls cell shape and directs actin stress fiber formation and focal adhesion alignment in spreading cells. *PLoS One* 8, e77328.
- Guha M, Zhou M, Wang YL (2005). Cortical actin turnover during cytokinesis requires myosin II. *Curr Biol* 15, 732–736.
- Haviv L, Gillo D, Backouche F, Bernheim-Groswasser A (2008). A cytoskeletal demolition worker: myosin II acts as an actin depolymerization agent. *J Mol Biol* 375, 325–330.
- Hayakawa K, Tatsumi H, Sokabe M (2011). Actin filaments function as a tension sensor by tension-dependent binding of cofilin to the filament. *J Cell Biol* 195, 721–727.
- Hayakawa K, Tatsumi H, Sokabe M (2012). Mechano-sensing by actin filaments and focal adhesion proteins. *Commun Integr Biol* 5, 572–577.
- Higashida C, Kiuchi T, Akiba Y, Mizuno H, Maruoka M, Narumiya S, Mizuno K, Watanabe N (2013). F- and G-actin homeostasis regulates mechano-sensitive actin nucleation by formins. *Nat Cell Biol* 15, 395–405.
- Higashida C, Miyoshi T, Fujita A, Oceguera-Yanez F, Monypenny J, Andou Y, Narumiya S, Watanabe N (2004). Actin polymerization-driven molecular movement of mDia1 in living cells. *Science* 303, 2007–2010.
- Hoffman LM, Jensen CC, Chaturvedi A, Yoshigi M, Beckerle MC (2012). Stretch-induced actin remodeling requires targeting of zyxin to stress fibers and recruitment of actin regulators. *Mol Biol Cell* 23, 1846–1859.
- Jurado C, Haserick JR, Lee J (2005). Slipping or gripping? Fluorescent speckle microscopy in fish keratocytes reveals two different mechanisms for generating a retrograde flow of actin. *Mol Biol Cell* 16, 507–518.
- Kaunas R, Nguyen P, Usami S, Chien S (2005). Cooperative effects of Rho and mechanical stretch on stress fiber organization. *Proc Natl Acad Sci USA* 102, 15895–15900.
- Kolega J (2004). Phototoxicity and photoinactivation of blebbistatin in UV and visible light. *Biochem Biophys Res Commun* 320, 1020–1025.
- Kondo T, Isoda R, Uchimura T, Sugiyama M, Hamao K, Hosoya H (2012). Di-phosphorylated but not monophosphorylated myosin II regulatory light chain localizes to the midzone without its heavy chain during cytokinesis. *Biochem Biophys Res Commun* 417, 686–691.
- Leopoldt D, Yee HF Jr, Rozengurt E (2001). Calyculin-A induces focal adhesion assembly and tyrosine phosphorylation of p125(Fak), p130(Cas), and paxillin in Swiss 3T3 cells. *J Cell Physiol* 188, 106–119.
- Lomakin AJ, Lee KC, Han SJ, Bui DA, Davidson M, Mogilner A, Danuser G (2015). Competition for actin between two distinct F-actin networks

- defines a bistable switch for cell polarization. *Nat Cell Biol* 17, 1435–1445.
- Medeiros NA, Burnette DT, Forscher P (2006). Myosin II functions in actin-bundle turnover in neuronal growth cones. *Nat Cell Biol* 8, 215–226.
- Mitchison T, Kirschner M (1988). Cytoskeletal dynamics and nerve growth. *Neuron* 1, 761–772.
- Mizuno H, Tanaka K, Yamashiro S, Narita A, Watanabe N (2018). Helical rotation of the diaphanous-related formin mDia1 generates actin filaments resistant to cofilin. *Proc Natl Acad Sci USA* 115, E5000–E5007.
- Morishita Y, Tsutsumi K, Ohta Y (2015). Phosphorylation of serine 402 regulates RacGAP protein activity of FilGAP protein. *J Biol Chem* 290, 26328–26338.
- Murrell MP, Gardel ML (2012). F-actin buckling coordinates contractility and severing in a biomimetic actomyosin cortex. *Proc Natl Acad Sci USA* 109, 20820–20825.
- Murthy K, Wadsworth P (2005). Myosin-II-dependent localization and dynamics of F-actin during cytokinesis. *Curr Biol* 15, 724–731.
- Murugesan S, Hong J, Yi J, Li D, Beach JR, Shao L, Meinhardt J, Madison G, Wu X, Betzig E, Hammer JA (2016). Formin-generated actomyosin arcs propel T cell receptor microcluster movement at the immune synapse. *J Cell Biol* 215, 383–399.
- Nishida E, Iida K, Yonezawa N, Koyasu S, Yahara I, Sakai H (1987). Cofilin is a component of intranuclear and cytoplasmic actin rods induced in cultured cells. *Proc Natl Acad Sci USA* 84, 5262–5266.
- Okimura C, Iwadate Y (2016). Hybrid mechanosensing system to generate the polarity needed for migration in fish keratocytes. *Cell Adh Migr* 10, 406–418.
- Ream RA, Theriot JA, Somero GN (2003). Influences of thermal acclimation and acute temperature change on the motility of epithelial wound-healing cells (keratocytes) of tropical, temperate and Antarctic fish. *J Exp Biol* 206, 4539–4551.
- Reymann AC, Boujemaa-Paterski R, Martiel JL, Guerin C, Cao W, Chin HF, De La Cruz EM, They M, Blanchoin L (2012). Actin network architecture can determine myosin motor activity. *Science* 336, 1310–1314.
- Romet-Lemonne G, Jegou A (2013). Mechanotransduction down to individual actin filaments. *Eur J Cell Biol* 92, 333–338.
- Sakamoto T, Limouze J, Combs CA, Straight AF, Sellers JR (2005). Blebbistatin, a myosin II inhibitor, is photoinactivated by blue light. *Biochemistry* 44, 584–588.
- Schaub S, Bohnet S, Laurent VM, Meister JJ, Verkhovsky AB (2007). Comparative maps of motion and assembly of filamentous actin and myosin II in migrating cells. *Mol Biol Cell* 18, 3723–3732.
- Shirinsky VP, Antonov AS, Birukov KG, Sobolevsky AV, Romanov YA, Kabaeva NV, Antonova GN, Smirnov VN (1989). Mechano-chemical control of human endothelium orientation and size. *J Cell Biol* 109, 331–339.
- Small JV (1995). Getting the actin filaments straight: nucleation-release or treadmilling? *Trends Cell Biol* 5, 52–55.
- Smith MB, Kiuchi T, Watanabe N, Vavylonis D (2013). Distributed actin turnover in the lamellipodium and FRAP kinetics. *Biophys J* 104, 247–257.
- Straight AF, Cheung A, Limouze J, Chen I, Westwood NJ, Sellers JR, Mitchison TJ (2003). Dissecting temporal and spatial control of cytokinesis with a myosin II inhibitor. *Science* 299, 1743–1747.
- Svitkina TM, Verkhovsky AB, McQuade KM, Borisy GG (1997). Analysis of the actin-myosin II system in fish epidermal keratocytes: mechanism of cell body translocation. *J Cell Biol* 139, 397–415.
- Tardy Y, McGrath JL, Hartwig JH, Dewey CF (1995). Interpreting photoactivated fluorescence microscopy measurements of steady-state actin dynamics. *Biophys J* 69, 1674–1682.
- Theriot JA, Mitchison TJ (1991). Actin microfilament dynamics in locomoting cells. *Nature* 352, 126–131.
- Valloton P, Gupton SL, Waterman-Storer CM, Danuser G (2004). Simultaneous mapping of filamentous actin flow and turnover in migrating cells by quantitative fluorescent speckle microscopy. *Proc Natl Acad Sci USA* 101, 9660–9665.
- Vogel SK, Petrasek Z, Heinemann F, Schwille P (2013). Myosin motors fragment and compact membrane-bound actin filaments. *Elife* 2, e00116.
- Watanabe N (2010). Inside view of cell locomotion through single-molecule: fast F-/G-actin cycle and G-actin regulation of polymer restoration. *Proc Jpn Acad Ser B Phys Biol Sci* 86, 62–83.
- Watanabe N (2012). Fluorescence single-molecule imaging of actin turnover and regulatory mechanisms. *Methods Enzymol* 505, 219–232.
- Watanabe N, Mitchison TJ (2002). Single-molecule speckle analysis of actin filament turnover in lamellipodia. *Science* 295, 1083–1086.
- Watanabe S, Ando Y, Yasuda S, Hosoya H, Watanabe N, Ishizaki T, Narumiya S (2008). mDia2 induces the actin scaffold for the contractile ring and stabilizes its position during cytokinesis in NIH 3T3 cells. *Mol Biol Cell* 19, 2328–2338.
- Watanabe TM, Sato T, Gonda K, Higuchi H (2007). Three-dimensional nanometry of vesicle transport in living cells using dual-focus imaging optics. *Biochem Biophys Res Commun* 359, 1–7.
- Wilson CA, Tsuchida MA, Allen GM, Barnhart EL, Applegate KT, Yam PT, Ji L, Keren K, Danuser G, Theriot JA (2010). Myosin II contributes to cell-scale actin network treadmill through network disassembly. *Nature* 465, 373–377.
- Yamashiro S, Mizuno H, Smith MB, Ryan GL, Kiuchi T, Vavylonis D, Watanabe N (2014). New single-molecule speckle microscopy reveals modification of the retrograde actin flow by focal adhesions at nanometer scales. *Mol Biol Cell* 25, 1010–1024.
- Yamashiro S, Mizuno H, Watanabe N (2015). An easy-to-use single-molecule speckle microscopy enabling nanometer-scale flow and wide-range lifetime measurement of cellular actin filaments. *Methods Cell Biol* 125, 43–59.
- Yamashiro S, Watanabe N (2017). Overview of single-molecule speckle (SiMS) microscopy and its electroporation-based version with efficient labeling and improved spatiotemporal resolution. *Sensors (Basel)* 17, 1585.
- Yi J, Wu XS, Crites T, Hammer JA 3rd (2012). Actin retrograde flow and actomyosin II arc contraction drive receptor cluster dynamics at the immunological synapse in Jurkat T cells. *Mol Biol Cell* 23, 834–852.